

Cascade of magnetic field induced Lifshitz transitions in the ferromagnetic Kondo lattice material YbNi_4P_2

H. Pfau,^{1,2} R. Daou,³ S. Friedemann,⁴ S. Karbassi,⁴ S. Ghannadzadeh,⁵ R. K  chler,¹ S. Hamann,¹
A. Steppke,¹ D. Sun,¹ M. K  nig,¹ A. P. Mackenzie,^{1,6} K. Kliemt,⁷ C. Krellner,⁷ and M. Brando¹

¹*Max Planck Institute for Chemical Physics of Solids, D-01187 Dresden, Germany*

²*Stanford Institute for Materials and Energy Sciences, SLAC National Accelerator Laboratory,
2575 Sand Hill Road, Menlo Park, California 94025, USA*

³*Normandie Univ, ENSICAEN, UNICAEN, CNRS, CRISMAT, 14000 Caen, France.*

⁴*HH Wills Laboratory, University of Bristol, BS8 1TL Bristol, UK*

⁵*High Field Magnet Laboratory, University of Nijmegen, 6525 ED Nijmegen, The Netherlands*

⁶*Scottish Universities Physics Alliance (SUPA), School of Physics and Astronomy,
University of St. Andrews, St. Andrews KY16 9SS, United Kingdom*

⁷*Physikalisches Institut, Johann Wolfgang Goethe-Universit  t, D-60438 Frankfurt am Main, Germany*

(Dated: December 20, 2016)

We have studied the magnetic field dependence of transport and thermodynamic properties of the Kondo lattice compound YbNi_4P_2 for fields up to 30 T. On top of a continuous suppression of the Kondo effect with increasing field we identify nine Lifshitz transitions between 0.4 and 18 T. Using a detailed analysis of the measured transport coefficients, we were able to identify in most cases the type of Lifshitz transition being of neck or void type. This large number of Lifshitz transitions observed within this small energy window is unprecedented and is the result of the particular flat renormalized band structure with strong $4f$ -electron character shaped by the Kondo lattice effect which acts not just on a single, but on multiple bands.

The topology of the Fermi surface plays a key role in understanding metallic materials, because their electronic properties are determined by thermally excited quasiparticles confined to a narrow window around the Fermi energy. Angle-resolved photoemission spectroscopy (ARPES) and quantum oscillation (QO) measurements are the most common tools to determine the Fermi surface. While ARPES relies on an excellent surface quality, QOs need to be performed at high magnetic fields of the order of 10 T but are typically interpreted using band structure calculations at zero field. The ability of QOs to interpret zero field properties is therefore under intense discussion, *e.g.* in high-temperature superconductors [1–5] and low-carrier-density topological materials with surface states [6].

The above considerations are especially relevant to Kondo lattice systems in which local f -electrons and conduction electrons form composite heavy quasiparticles below the Kondo temperature T_K . Due to the coherence effects in the lattice, these systems develop flat bands close to the Fermi level and van-Hove singularities in the renormalized density of state (DOS) [7]. The Kondo energy scale $k_B T_K$ is a measure of the Fermi energy of heavy fermion systems. Since it roughly corresponds to a Zeeman energy $\frac{1}{2} g_{\text{eff}} \mu_B B$ for magnetic fields around 10 T, they are very susceptible to Fermi surface changes due to magnetic field induced Lifshitz transitions (LTs): changes in the topology of the Fermi surface without symmetry breaking. [8]. Because of the strong correlations and the specific crystalline electric field (CEF) ground state, it is particularly difficult to predict the exact field strengths at which those LTs will take place [9].

LTs have been reported in heavy fermion (HF) compounds such as YbRh_2Si_2 [10–13] and CeIrIn_5 [14], near the metamagnetic transition in CeRu_2Si_2 [15–17] and in the hidden ordered phase of URu_2Si_2 [18, 19]. They are also discussed in connection with superconductivity, *e.g.* in metamagnetic ferromagnets [20–22], URhGe [23], Sr_2RuO_4 [24] and in high-temperature superconductors [1, 2]. Hence, LTs are an integral part of the complex phase diagram of correlated materials. Additionally, LTs are also relevant in topological systems, for example in Dirac semimetals [6].

In this paper we study YbNi_4P_2 , which has a quasi-1D crystal structure with isolated chains of magnetic Yb^{3+} atoms along the crystallographic c -axis [25]. The quasi 1D character leads to flat sheets in two major Fermi surfaces in the uncorrelated band structure calculations, in which Ni-3d states dominate the density of states [26, 27]. YbNi_4P_2 is a Kondo lattice with $T_K = 8$ K, which orders ferromagnetically at $T_C \approx 0.15$ K. While the FM state is suppressed at $B_c \approx 0.06$ T applied along the c -axis [27], YbNi_4P_2 can also be tuned towards a ferromagnetic (FM) quantum critical point (QCP) by As-substitution [26, 27]. Such a FM QCP was thought not to exist in metallic systems [28, 29] and is believed to be realized in YbNi_4P_2 due to its 1D-character [27]. It is therefore very important to experimentally determine the Fermi surface and verify its low-dimensional character.

While ARPES measurements were not successful so far due to difficulties to cleave YbNi_4P_2 crystals, there are also no QOs available to date. Additionally, the latter method suffers from the afore mentioned difficulties in their interpretation. Recent studies on YbRh_2Si_2

demonstrated that combining magnetic field dependent thermopower, resistivity and magnetostriction measurements provides a powerful toolset to detect changes in the Fermi surface due to field induced LTs [12, 13]. It also allows studies in a magnetic field range below the fields necessary for QO measurements. Using this tool set, we show how a relatively small external magnetic field dramatically modifies the Fermi surface of the HF system YbNi₄P₂ producing in total nine LTs.

While the comparison with renormalized band structure calculations proved to be very successful to also determine the type of Fermi surface changes in YbRh₂Si₂ [9, 12, 30], such calculations are not yet available for YbNi₄P₂. Therefore, we have extended our analysis of the thermopower and resistivity to compare the observed signatures to general theoretical predictions for transport coefficients close to a LT. This analysis enables us not only to identify the position of the LTs, but also to determine their topological character and carrier type. Similar to YbRh₂Si₂, the topological changes lie on top of an overall continuous suppression of the Kondo effect which is reflected in the continuous decrease of the effective mass m^* with increasing field [12, 31]. Our study indicates that the observation of several Zeeman-driven LTs on top of a smooth suppression of the Kondo effect in magnetic field is a generic property of Kondo lattice systems.

Our measurements on single crystalline samples [32] focus on a magnetic field $B \parallel c$ above B_c , which suppresses the ferromagnetic order. We performed resistivity measurements on two samples with current $I \parallel c$. Sample #1 has a residual resistivity $\rho_0 \approx 1 \mu\Omega\text{cm}$ and was measured in magnetic fields up to 30 T at the High Field Magnet Laboratory in Nijmegen. Sample #2 with $\rho_0 \approx 1.7 \mu\Omega\text{cm}$ was cut from sample #4 and shaped into a thin wire using a focussed ion beam (FIB) patterning. It was used for resistivity measurements in a dilution refrigerator down to 30 mK and in fields up to 18 T. We checked that the FIB patterning did not alter the resistivity of the sample. A third sample #3 with $\rho_0 \approx 2.6 \mu\Omega\text{cm}$ was used for thermal transport measurements up to 12 T using a standard one-heater-two-thermometer configuration. Magnetostriction was measured up to 10 T on the largest sample #4 (length $L = 2 \text{ mm}$) by means of a high-resolution capacitive CuBe dilatometer [33].

Figure 1(a) presents the resistivity $\rho(B)$ of samples #1 and #2. Both samples show the same overall behavior: At small magnetic fields $B \leq 1 \text{ T}$, we observe a negative magnetoresistance, which is typical for Kondo systems. It indicates the suppression of spin-flip scattering and hence a suppression of the Kondo effect. Above $B_c \approx 0.06 \text{ T}$, we observe several kinks in $\rho(B)$ at the positions $B_i, i = 1 \dots 9$, which are determined from $\rho(B)$ of sample #2. We list them in Tab. I and marked them with gray vertical lines in Fig. 1. In some cases they are associated with a strong change of slope, e.g., at

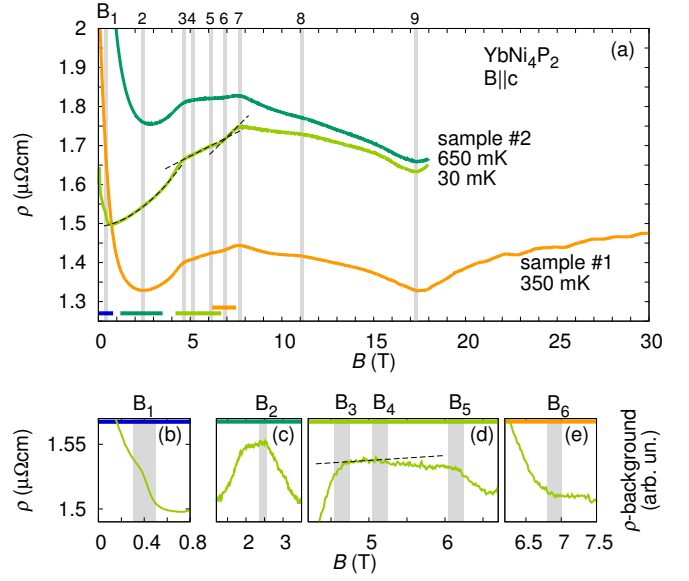


FIG. 1. Resistivity. (a) Resistivity $\rho(B)$ as a function of magnetic field B up to 30 T. (b) A zoom into the region around B_1 . (c)-(e) Background subtracted resistivity for three different field ranges to highlight the signatures of the transitions $B_{2..6}$. The background determined from a linear (d,e) or quadratic (c) fit to the data is shown in (a) as dashed lines. Dashed line in (d) is a guide to the eye to highlight the changes around B_4 . The field intervals for (b)-(e) are marked with solid bars on the bottom of (a). Gray vertical lines represent the transition fields $B_i, i = 1 \dots 9$, their thickness corresponds to the error of B_i .

7.7 T and 17.5 T, while for others we used the expanded scale of Fig. 1(b)-(e) to highlight their weaker, but distinct, signatures. Importantly, the position of these kinks is temperature independent, suggesting Lifshitz transitions as their origin. At approximately 15 T we start to observe quantum oscillations which are clearly seen at higher fields and will be discussed in detail elsewhere.

To study the nature of these transitions, we plot in Fig. 2(a) the thermopower as $S(B)/T$. At zero field, $S(B)/T$ varies strongly with temperature, which can be related to the strong fluctuations in the vicinity of the QCP in YbNi₄P₂. In finite field, $S(B)/T$ exhibits several extrema up to 12 T and the strong field dependence indicates the presence of several field induced transitions. By marking the fields B_i of the kinks seen in $\rho(B)$ with gray lines, we notice that $S(B)/T$ shows a complex response connected to an inflection point and an extremum close to B_i .

Figure 2(b) shows a measurement of the linear magnetostriction coefficient $\lambda(B) = \partial(\Delta L(B)/L)/\partial B$ along the c -axis at 50 mK. This quantity changes sign across $B_c \approx 0.06 \text{ T}$ [27], which is a clear signature of a symmetry breaking phase transition. At fields larger than B_c , $\lambda(B)$ shows distinct kinks at B_i . However, it always

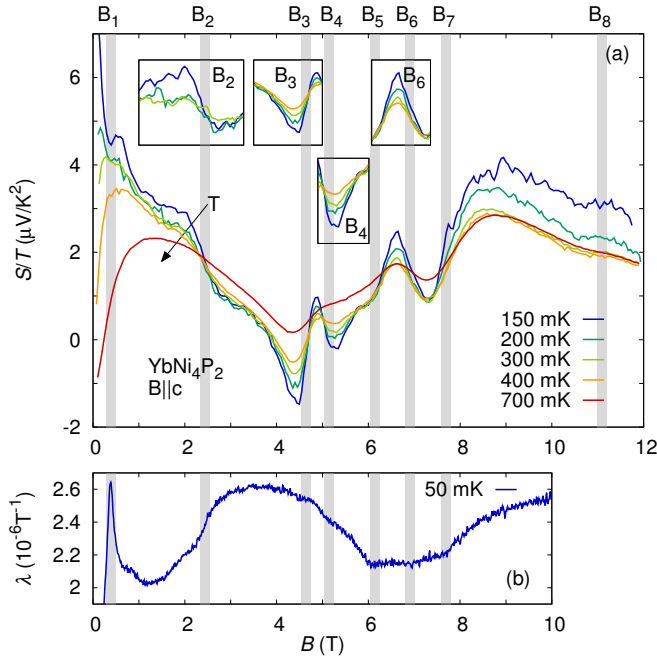


FIG. 2. Thermopower and magnetostriction. (a) The main panel shows the thermopower $S(B, T)$ of sample #3 plotted as $S(B)/T$ as a function of B . Small insets are selective views of the signatures of the transitions at $B_{2,3,4,6}$. A background estimated from the data at 400 mK was subtracted for inset at B_2 for an easier comparison with theory (see text). (b) Linear magnetostriction coefficient $\lambda(B)$ of sample #4 as a function of B . Gray vertical lines represent the transition fields B_i , $i = 1 \dots 9$ determined from $\rho(B)$, their thickness corresponds to the error of B_i .

stays positive for $0.06 < B \leq 10$ T and does not change sign, which rules out further symmetry-breaking transitions and suggests the presence of LTs at these fields [8, 34]. This finding is corroborated by results of specific heat measurements: Except for the ferromagnetic phase transition at 150 mK ($B = 0$), there is no sign for another finite temperature phase transition at higher fields ($B \parallel c$) in the temperature dependence of the specific heat, measured between 60 mK and 4 K for several fields up to 12 T [35]. Furthermore, no significant enhancement of the magnetization $M(B)$ is observed across B_i (not shown).

To investigate, if the ground state of YbNi_4P_2 is a Fermi liquid, we measured the temperature dependence of $\rho(T)$, which indeed follows the Fermi liquid form $\rho(T) = \rho_0 + AT^2$ at all B_i (not shown). This indicates that the LTs are not associated with anomalous or quantum critical behavior, as sometimes observed in metamagnetic systems like in CeRu_2Si_2 [15]. Having established the Fermi liquid ground state, we can study the field evolution of the effective mass m^* using the relation $m^*(B) \propto \sqrt{A(B)} \propto \chi(B) \propto \gamma(B) \propto \text{DOS}(B)$. Here, A is the quasiparticle-quasiparticle scattering rate

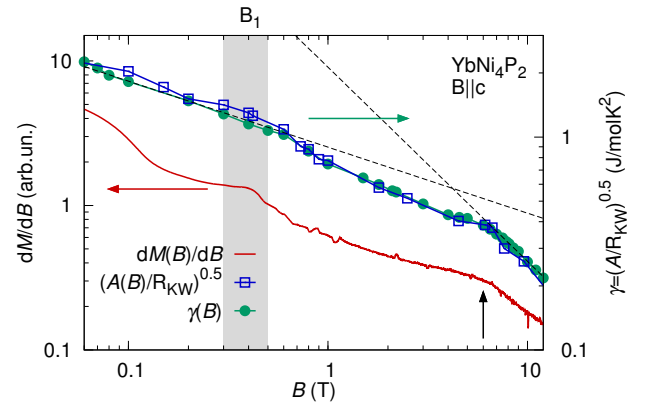


FIG. 3. Field dependence of the effective mass above B_c . As a measure of the effective mass, we plot here the field derivative of the magnetization dM/dB , the specific heat coefficient $\gamma(B)$ and the square root of the A coefficient of the resistivity in a double-logarithmic plot. All three quantities show the same behavior in field. The dashed lines highlight the change of slope in $\gamma(B)$ just above B_1 (gray line) and around $B_5 < B < B_7$ (short arrow). The changes around the latter field scale are too broad in our measurements to be connected to a single B_i .

extracted from the T^2 term in $\rho(B)$, χ is the magnetic susceptibility, $\gamma(B)$ the Sommerfeld coefficient. All four quantities should be proportional to the density of states DOS. Fig. 3 shows $\gamma(B)$, $\chi(B)$ and $\sqrt{A(B)/R_{\text{KW}}}$, where R_{KW} is the Kadowaki-Woods ratio, which we determined to be $2 \mu\Omega \text{ cm}/(\text{J/molK}^2)^2$ in YbNi_4P_2 . All three quantities demonstrate, that m^* decreases strongly but continuously between 0.06 T and 10 T. Above 10 T, m^* is still about 0.2 J/molK^2 , which confirms the persistence of the Kondo lattice effect even at this high field. Similar behavior was observed in YbRh_2Si_2 [12]. Interestingly, m^* shows significant changes of slope only at certain B_i , i.e., at B_1 and around $B_5 < B < B_7$.

Now, we use the strong signatures in S/T together with the fine structure seen in ρ to try to extract the type of LT at all B_i . There are two main types as displayed in Fig. 4(c),(d): the void type where a Fermi surface sheet vanishes, and a neck type where a Fermi surface splits into two sheets. Following the terminology of Ref. [34, 36], the side of the transition where the new pocket is absent and where the neck is not broken corresponds to region I. Figures 4(a)-(d) present theoretical predictions for the signatures one expects to observe in electrical conductivity σ and thermopower at a LT [34, 36, 37]. Such signatures were already observed experimentally across LTs in several different systems, e.g., in elements and metallic solid solutions [36, 38], semiconductors [36, 39] and high-temperature superconductors [40, 41]. However, these materials need to be tuned to the LT by external pressure or doping which in most

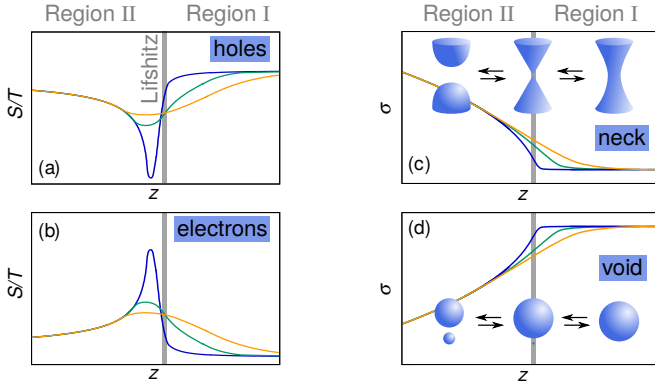


FIG. 4. Lifshitz transitions. Panels (a)-(d) present theoretical calculations of the signatures in thermopower S and conductivity σ close to a Lifshitz transition tuned by some parameter z . The plots are reproduced from [34, 36] for the clean case and presented for three different temperatures. The sign of the thermopower signature (maximum or minimum) is defined by the type of charge carrier. The sign of the conductivity, (i.e., minimum or maximum in $\partial^2 \sigma / \partial z^2$), is defined by the type of Lifshitz transition, i.e., either neck or void type [36].

cases corresponds to a much higher energy shift compared to the shift due to magnetic fields of the order of a few tesla. In contrast to thermodynamic quantities, transport properties such as resistivity and thermopower are most affected by changes in the scattering time and not the density of states close to a LT and usually show a stronger response. The same transport properties can also determine the type of LT (using the conductivity σ), the carrier type involved (using S/T), and its direction, i.e., which side of the transition corresponds to region I and which one to region II (from asymmetry in S/T) [36]. These signatures are independent of the specific band structure.

Some transitions are difficult to analyze in this way due to the strong B -dependent background (B_1), a relatively large noise level at high fields (B_8) and the limited field range for the thermopower measurement (B_9). For $S(B)/T$, we highlight the signatures in the insets in Fig. 2 for a direct comparison with Fig. 4(a),(b). For the conductivity, we assume $\sigma = 1/\rho$ and a negligible contribution from the Hall resistivity for simplicity and compare Fig. 1 with Fig. 4(c),(d). We consider for example the transition at B_3 : i) The peak in S/T is at fields smaller than B_3 , corresponding to region II; ii) the peak is negative, suggesting that hole carriers are dominant; iii) the slope of $\rho(B)$ decreases for $B > B_3$, so the transition is of neck type. Hence a neck joins two pockets of a hole band as the field increases, crossing B_3 . In a similar way we can identify the characteristics of the other transitions, which we summarize in Tab. I.

While the transitions at $B_{1,8,9}$ are difficult to analyze as explained before, those at B_5 and B_7 show a distinctly

	B_1	B_2	B_3	B_4	B_5	B_6	B_7	B_8	B_9
$B(T)$	0.40	2.45	4.65	5.15	6.15	6.90	7.70	11.0	17.5
type		neck	neck	neck	neck	void	neck	neck	void
carr. type		e	h	h	*	e	*		
direction		II→I	II→I	I→II	*	II→I	*		

TABLE I. Field value and characteristics of the Lifshitz transitions determined from a direct comparison of the shape of $\rho(B)$ from Fig. 1 and $S(B)/T$ from Fig. 2 with theoretical predictions shown in Fig. 4. The error of B_i is 0.1 T. No statement can be made in cases, where the signatures are covered by a large background (B_1) large noise (B_8) or when the accessible field range is too small (B_9). *: The deviation from the prediction in $S(B)/T$ for B_5 and B_7 hints towards an involvement of the flat Fermi surface sheets (see text). e: electronic; h: hole; I(II): region I(II) (see Fig. 4)

different shape of $S(B)/T$ compared to the prediction in Fig. 4. Special symmetry cases, e.g., transitions in lower dimensions, are expected to produce different transport signals [34, 42]. Additionally, we observe stronger responses in the magnetostriction coefficient and in m^* in this field range and for B_1 compared to the other LTs. The DOS is expected to show stronger signatures in the case of low-dimensional Fermi surfaces [34, 42]. Interestingly, the uncorrelated band structure calculations predict two quasi-1D Fermi surface sheets in the k_x - k_y plane due to the one-dimensional character of the crystal structure [26]. These flat sheets can also undergo a LT, which might explain the strong features in λ and m^* and the different shape in S/T compared to the other transitions. Hence, B_1 , B_5 and B_7 may be connected to LTs in the renormalized quasi-1D Fermi surface sheets of YbNi_4P_2 .

Our results also shed light on a further strongly discussed topic in Kondo lattice systems: Namely, whether on crossing the QCP from the paramagnetic to the magnetically ordered phase, the Fermi volume loses the f -electron right at the QCP (Kondo breakdown scenario) or well within the magnetically ordered regime (spin density wave (SDW) scenario) [43–47] YbNi_4P_2 is located slightly on the magnetically ordered side of the QCP [27], thus just in a regime where the Kondo breakdown and the SDW scenario makes opposite predictions. Our results demonstrate that the Fermi surface is extremely sensitive to small external fields of the order of 1 T. This implies the presence of weakly dispersing bands, which are shifted by the Zeeman splitting on a significant portion of the Brillouin zone. This is a strong indication that the f degrees of freedom are involved in the formation of the Fermi surfaces in the field range $B > B_c$, which was investigated in this study. Thus our results hint towards the SDW scenario.

In conclusion, we have investigated the Kondo lattice system YbNi_4P_2 in magnetic fields above its ferromagnetic order. We observe a gradual suppression of the Kondo effect reflected in the suppression of the effective

mass with increasing magnetic field. On top of this effect, we discovered in total nine field induced LTs between 0.4 T and 18 T. With the help of a detailed analysis of the transport properties, we were able to identify the specific type of LTs being of void or neck type and the carrier type involved. It also allowed us to find indications for the existence of Fermi surfaces with a lower dimension, which is an important step towards an understanding of the FM QCP in YbNi_4P_2 . Our analysis yields information about the bandstructure and its changes without involving specific band structure calculations and hence serves as a benchmark for future theoretical models such as RBS calculations.

The large number of Lifshitz transitions in a small magnetic field range reveals the presence of many extrema in the band structure of YbNi_4P_2 very close to the Fermi level, shaped by the Kondo lattice effect with anisotropic momentum-dependent hybridization acting in a multiband system. The magnetic field scale of the transitions is therefore to first order determined by the Kondo temperature $T_K = 8$ K and to second order by the specifics of the hybridization and the multiband character. The comparison to other Kondo lattice systems such as YbRh_2Si_2 suggests that this is a generic property of heavy fermion systems.

We are indebted to C. Geibel, A. Gourgout, F. Steglich and A. A. Varlamov for useful discussions. This work was supported by the German Research Foundation (DFG) through the grants BR4110/1-1 and KR3831/4-1. H.P. acknowledges the support from the Alexander von Humboldt Foundation.

-
- [1] C. Liu, T. Kondo, R. M. Fernandes, A. D. Palczewski, E. D. Mun, N. Ni, A. N. Thaler, A. Bostwick, E. Rotenberg, J. Schmalian, S. L. Budko, P. C. Canfield, and A. Kaminski, *Nat. Phys.* **6**, 419 (2010).
 - [2] D. LeBoeuf, N. Doiron-Leyraud, B. Vignolle, M. Sutherland, B. J. Ramshaw, J. Levallois, R. Daou, F. Laliberte, O. Cyr-Choiniere, J. Chang, Y. J. Jo, L. Balicas, R. Liang, D. A. Bonn, W. N. Hardy, C. Proust, and L. Taillefer, *Phys. Rev. B* **83**, 054506 (2011).
 - [3] N. Doiron-Leyraud, C. Proust, D. LeBoeuf, J. Levallois, J.-B. Bonnemaison, R. Liang, D. A. Bonn, W. N. Hardy, and L. Taillefer, *Nature* **447**, 565 (2007).
 - [4] N. Barisic, S. Badoux, M. K. Chan, C. Dorow, W. Tabis, B. Vignolle, G. Yu, J. Beard, X. Zhao, C. Proust, and M. Greven, *Nat Phys* **9**, 761 (2013).
 - [5] G. Grissonnanche, F. Laliberte, S. Dufour-Beausejour, A. Riopel, S. Badoux, M. Caouette-Mansour, M. Matysiak, A. Juneau-Fecteau, P. Bourgeois-Hope, O. Cyr-Choiniere, J. C. Baglo, B. J. R. R. L. D. A. Bonn, W. N. Hardy, S. Kramer, D. LeBoeuf, D. Graf, N. Doiron-Leyraud, and L. Taillefer, *arXiv:1508.05486*.
 - [6] S.-Y. Xu, C. Liu, I. Belopolski, S. K. Kushwaha, R. Sankar, J. W. Krizan, T.-R. Chang, C. M. Polley, J. Adell, T. Balasubramanian, K. Miyamoto, N. Ali-doust, G. Bian, M. Neupane, H.-T. Jeng, C.-Y. Huang, W.-F. Tsai, T. Okuda, A. Bansil, F. C. Chou, R. J. Cava, H. Lin, and M. Z. Hasan, *Phys. Rev. B* **92**, 075115 (2015).
 - [7] A. C. Hewson, *The Kondo Problem to Heavy Fermions* (Cambridge University Press, Cambridge, England, 1993).
 - [8] I. Lifshitz, *Sov. Phys. JETP-USSR* **11**, 1130 (1960).
 - [9] G. Zwicknagl, *Journal of Physics: Condensed Matter* **23**, 094215 (2011).
 - [10] Y. Tokiwa, P. Gegenwart, T. Radu, J. Ferstl, G. Sparn, C. Geibel, and F. Steglich, *Phys. Rev. Lett.* **94**, 226402 (2005).
 - [11] P. M. C. Rourke, A. McCollam, G. Lapertot, G. Knebel, J. Flouquet, and S. R. Julian, *Phys. Rev. Lett.* **101**, 237205 (2008).
 - [12] H. Pfau, R. Daou, S. Lausberg, H. R. Naren, M. Brando, S. Friedemann, S. Wirth, T. Westerkamp, U. Stockert, P. Gegenwart, C. Krellner, C. Geibel, G. Zwicknagl, and F. Steglich, *Phys. Rev. Lett.* **110**, 256403 (2013).
 - [13] A. Pourret, G. Knebel, T. D. Matsuda, G. Lapertot, and J. Flouquet, *J. Phys. Soc. Jpn.* **82**, 053704 (2013).
 - [14] D. Aoki, G. Seyfarth, A. Pourret, A. Gourgout, A. McCollam, J. A. N. Bruin, Y. Krupko, and I. Sheikin, *Phys. Rev. Lett.* **116**, 037202 (2016).
 - [15] R. Daou, C. Bergemann, and S. R. Julian, *Phys. Rev. Lett.* **96**, 026401 (2006).
 - [16] H. Pfau, R. Daou, M. Brando, and F. Steglich, *Phys. Rev. B* **85**, 035127 (2012).
 - [17] M. Boukahil, A. Pourret, G. Knebel, D. Aoki, Y. Ōnuki, and J. Flouquet, *Phys. Rev. B* **90**, 075127 (2014).
 - [18] M. M. Altarawneh, N. Harrison, S. E. Sebastian, L. Balicas, P. H. Tobash, J. D. Thompson, F. Ronning, and E. D. Bauer, *Phys. Rev. Lett.* **106**, 146403 (2011).
 - [19] L. Malone, T. D. Matsuda, A. Antunes, G. Knebel, V. Taufour, D. Aoki, K. Behnia, C. Proust, and J. Flouquet, *Phys. Rev. B* **83**, 245117 (2011).
 - [20] H. Kotegawa, V. Taufour, D. Aoki, G. Knebel, and J. Flouquet, *J. Phys. Soc. Jpn.* **80**, 083703 (2011).
 - [21] Y. Yamaji, T. Misawa, and M. Imada, *J. Phys. Soc. Jpn.* **76**, 063702 (2007).
 - [22] G. Bastien, A. Gourgout, D. Aoki, A. Pourret, I. Sheikin, G. Seyfarth, J. Flouquet, and G. Knebel, *Phys. Rev. Lett.* **117**, 206401 (2016).
 - [23] E. A. Yelland, J. M. Barraclough, W. Wang, K. V. Kamenev, and A. D. Huxley, *Nat. Phys.* **7**, 890 (2011).
 - [24] A. Steppke, L. Zhao, M. E. Barber, T. Scaffidi, F. Jerzembeck, H. Rosner, A. S. Gibbs, Y. Maeno, S. H. Simon, A. P. Mackenzie, and C. W. Hicks, *arXiv:1604.06669*.
 - [25] S. Députier, O. Pea, T. L. Bihan, J. Pivan, and R. Gurin, *Physica B: Condensed Matter* **233**, 26 (1997).
 - [26] C. Krellner, S. Lausberg, A. Steppke, M. Brando, L. Pedrero, H. Pfau, S. Tencé, H. Rosner, F. Steglich, and C. Geibel, *New J. Phys.* **13**, 103014 (2011).
 - [27] A. Steppke, R. Küchler, S. Lausberg, E. Lengyel, L. Steinke, R. Borth, T. Lühmann, C. Krellner, M. Nicklas, C. Geibel, F. Steglich, and M. Brando, *Science* **339**, 933 (2013).
 - [28] M. Brando, D. Belitz, F. M. Grosche, and T. R. Kirkpatrick, *Rev. Mod. Phys.* **88**, 025006 (2016).
 - [29] D. Belitz, T. R. Kirkpatrick, and T. Vojta, *Phys. Rev. Lett.* **82**, 4707 (1999).
 - [30] G. Zwicknagl, *Adv. Phys.* **41**, 203 (1992).

- [31] H. R. Naren, S. Friedemann, G. Zwicknagl, C. Krellner, C. Geibel, F. Steglich, and S. Wirth, *New J. Phys.* **15**, 093032 (2013).
- [32] K. Kliemt and C. Krellner, *Journal of Crystal Growth* **449**, 129 (2016).
- [33] R. K  chler, T. Bauer, M. Brando, and F. Steglich, *Review of Scientific Instruments* **83**, 095102 (2012).
- [34] Y. M. Blanter, M. I. Kaganov, A. V. Pantsulaya, and A. A. Varlamov, *Phys. Rep.* **245**, 159 (1994).
- [35] D. S. et al., To be published.
- [36] A. Varlamov, V. Egorov, and A. Pantsulaya, *Adv. Phys.* **38**, 469 (1989).
- [37] J. M. Buhmann and M. Sigrist, *Phys. Rev. B* **88**, 115128 (2013).
- [38] E. Bruno, B. Ginatempo, E. Guiliano, A. Ruban, and Y. Vekilov, *Physics Reports* **249**, 353 (1994).
- [39] J. F. Meng, N. V. Chandra Shekar, D.-Y. Chung, M. Kanatzidis, and J. V. Badding, *Journal of Applied Physics* **94**, 4485 (2003).
- [40] H. Hodovanets, Y. Liu, A. Jesche, S. Ran, E. D. Mun, T. A. Lograsso, S. L. Bud'ko, and P. C. Canfield, *Phys. Rev. B* **89**, 224517 (2014).
- [41] C. Shen, B. Si, C. Cao, X. Yang, J. Bao, Q. Tao, Y. Li, G. Cao, and Z.-A. Xu, *Journal of Applied Physics* **119**, 083903 (2016).
- [42] Y. M. Blanter, A. V. Pantsulaya, and A. A. Varlamov, *Phys. Rev. B* **45**, 6267 (1992).
- [43] Q. Si, M. S. Rabello, K. Ingersent, and J. L. Smith, *Nature* **413**, 804 (2001).
- [44] P. Gegenwart, Q. Si, and F. Steglich, *Nature Phys.* **4**, 186 (2008).
- [45] P. W  lfle and E. Abrahams, *Phys. Rev. B* **84**, 041101 (2011).
- [46] K. Kummer, S. Patil, A. Chikina, M. G  ttler, M. H  ppner, A. Generalov, S. Danzenb  cher, S. Seiro, A. Hannaske, C. Krellner, Y. Kucherenko, M. Shi, M. Radovic, E. Rienks, G. Zwicknagl, K. Matho, J. W. Allen, C. Laubschat, C. Geibel, and D. V. Vyalikh, *Phys. Rev. X* **5**, 011028 (2015).
- [47] S. Paschen, S. Friedemann, S. Wirth, F. Steglich, S. Kirchner, and Q. Si, *J. Magn. Magn. Mater.* **400**, 17 (2016).